

Modeling line-driven disk wind for broad absorption lines of quasars

Mariko NOMURA¹, Ken OHSUGA^{2, 3}, Keiichi WADA⁴, Hajime SUSA⁵, and Toru MISAWA^{2,6}

¹*Department of Physics, Ochanomizu University, 2-1-1 Otsuka, Bunkyo, Tokyo 112-8610*

²*National Astronomical Observatory of Japan, Osawa, Mitaka, Tokyo 181-8588*

³*School of Physical Sciences, Graduate University of Advanced Study (SOKENDAI), Shonan Village, Hayama, Kanagawa 240-0193*

⁴*Graduate School of Science and Engineering, Kagoshima University, Kagoshima 890-0065*

⁵*Department of Physics, Konan University, 8-9-1 Okamoto, Higashinadaku, Kobe*

⁶*School of General Education, Shinshu University, 3-1-1 Asahi, Matsumoto, Nagano 390-8621*

mariko@cosmos.phys.ocha.ac.jp, ken.ohsuga@nao.ac.jp, wada@astrophysics.jp, susa@konan-u.ac.jp, misawatr@shinshu-u.ac.jp

(Received 2012 October 11; accepted 2012 November 14)

Abstract

The disk wind, which is powered by the radiation force due to spectral lines (line force), is studied for broad absorption line (BAL) quasars. We investigate the structure of the disk wind based on the non-hydrodynamic method and compare with wind properties inferred from X-ray observations of BAL quasars. In this paper, we apply the stellar wind theory to the initial condition (the mass outflow rate at the base of the wind). We found the funnel-shaped winds with a half opening angle of $\sim 50^\circ$ for the case of $\epsilon = 0.3 - 0.9$ and $M_{\text{BH}} = 10^{7-8.5} M_\odot$, where ϵ is the Eddington ratio and M_{BH} is the black hole mass. Thus, the absorption features are observed for an observer of which a viewing angle is around 50° . A probability of BAL quasars is $\sim 7 - 11\%$, which is roughly consistent the abundance ratio of BAL quasars, $\sim 10 - 15\%$. Here, the probability is estimated by the solid angle, that the absorbing features would be detected, divided by 4π . In contrast, if the Eddington ratio is smaller than 0.01 or if the black hole is very massive, $M_{\text{BH}} \gtrsim 10^9 M_\odot$, the disk wind is not launched due to the less effective line force. Then, the quasars are identified as non-BAL quasars independently of the observer's viewing angle.

Key words: accretion: accretion disks — galaxies: active — methods: numerical — quasars: absorption lines — radiative transfer

1. Introduction

Accretion disks surrounding massive black holes are origins of activity of active galactic nuclei (AGNs). Their continuum emission comes from the disks and absorption as well as emission lines are thought to be produced by the matter above and/or around the disks. Broad absorption lines (BALs), of which line widths exceed $2,000 \text{ km s}^{-1}$, are observed in $\sim 10 - 20\%$ of quasars (Weymann et al. 1991; Hamann et al. 1993; Allen et al. 2011). The BALs are caused by metals moderately ionized and blueshifted with typical speeds of $\sim 10,000 \text{ km s}^{-1}$, up to $\sim 0.2c$ or more (e.g., Jannuzi et al. 1996). Weymann et al. (1991) suggested that the difference between the BAL and non-BAL quasars is caused by observers' viewing angles, since the properties of emission lines and continua of the BAL and non-BAL quasars are remarkably similar. Elvis (2000) proposed a phenomenological model of funnel-shaped disk wind, in which the matter is blown away toward the direction of the polar angle of $\sim 60 - 66^\circ$, to explain the abundance ratio of BAL quasars ($\sim 10\%$) via the viewing angle. If outflows launched from the surface of the accretion disks are accelerated toward the observer, the blueshift of the BALs could be explained. On the other hand, if the wind does not interrupt the line of sight, then BAL features would not emerge in the spectra.

Many theoretical models have been proposed to account for the origin of the outflows so far. One plausible scenario is that of ‘magnetically driven winds’ (Blandford & Payne 1982; Konigl & Kartje 1994; Everett & Murray 2007). In this model, the matter is magnetically accelerated. However, this model needs an extra mechanism to explain that the metals are moderately ionized, since the gas irradiated by the strong X-ray around the nucleus is fully photoionized (the so-called overionization problem).

Another plausible force that accelerates the disk wind is the radiation force due to spectral lines (line force). This model can explain both acceleration and ionization states. In this model, the gas on the surface of the accretion disk is accelerated by absorbing ultraviolet (UV) radiation from the disk through the bound-bound transition. Since the bound-bound absorption does not effectively occur for the overionized metals, the line force can accelerate the gas only in the lower-ionization state. Indeed, Stevens & Kallman (1990) showed that the line force works efficiently for the gas in the lower-ionization state and could be much more powerful than the radiation force due to electron scattering. Thus, though the luminosity of the disks in most quasars does not exceed the Eddington luminosity, the line-driven disk wind can be launched. The discovery of the line locking in the quasars (Foltz et al. 1987) strongly supports the idea that the line

force plays an important role in driving the outflows.

Proga et al. (1998, 1999) performed two-dimensional radiation-hydrodynamic (RHD) simulations of winds from disks around white dwarfs. This RHD method has been improved and applied to the disk winds in AGNs by Proga et al. (2000) and Proga & Kallman (2004) (hereafter PK04), in which the radiation transport of X-ray and UV is taken into consideration. They showed the funnel-shaped disk winds of which the opening angle is $\theta \sim 70^\circ$ where θ is the polar angle measured from the rotation axis. The line-driven wind is launched at the distance from the black hole of \sim several $100R_S$, where R_S is the Schwarzschild radius, and the ejected matter goes away mainly in the direction of $\theta \sim 70^\circ$. Their simulations revealed that the line-driven wind is in fact formed for a set of the black hole mass ($M_{\text{BH}} = 10^8 M_\odot$) and the Eddington ratio ($\epsilon = 0.5$). PK04 suggested that winds can be produced for $M_{\text{BH}} > 10^7 M_\odot$, but no winds appear for $\epsilon = 0.1$. This parameter dependence should be explored for a wider range of the parameters. Schurch et al. (2009) and Sim et al. (2010) calculated the spectra and compare them with those of the X-ray observations. However, they also only investigated the case of $\epsilon = 0.5$ and $M_{\text{BH}} = 10^8 M_\odot$.

Risaliti & Elvis (2010) studied the disk winds in AGNs for the wide parameter space of the black hole mass and the Eddington ratio. They investigated steady structures by non-hydrodynamic calculations, in which they solved the trajectories of the matter ejected from the disk surface without calculating the RHD equations. Their results seem to be consistent with the results of the RHD simulations. This non-hydrodynamic method is a powerful tool to investigate the dependence on several unknown parameters. Here, we use a similar method to investigate BAL quasars. However, Risaliti & Elvis (2010) did not research the wind properties, the ionization parameter, the velocity and the column density along the line of sight. Thus, within the framework of the non-hydrodynamic model, it is worth studying whether the disk wind explains the BAL features.

In Risaliti & Elvis (2010) and PK04, the density and the velocity at the base of the wind (at the disk surface) are treated as free parameters and simply assumed to be independent of the distance from the black hole. However, the stellar wind driven by the line force was investigated in detail. CAK75 derived the mass outflow rate (the density and the velocity) as functions of the gravity and the radiative flux. Thus, we should employ the mass outflow rate of the wind base consistent with the prediction of CAK75. Based on the CAK theory, the density at the wind base is not constant but decrease with distance from the black hole, if the velocity is assumed to be the sound velocity (see section 2.2).

In the present paper, employing the wide range of the parameters of the black hole mass, the Eddington ratio, we investigate the conditions under which the disk wind model can reproduce the X-ray absorption features of the BAL quasars. Although we do not study the spectra, we calculate the ionization parameter, the velocity and the column density for wide ϵ - M_{BH} range and compare them

with those inferred by the X-ray observation.

We describe our calculation method in §2. We present results in §3. Finally, §4 and §5 are devoted to discussion and conclusions.

2. Numerical Methods and Models

2.1. Outline

We study a steady structure of line-driven disk winds and apply them to the BAL quasars. We investigate the conditions under which the disk wind model can explain the X-ray absorption features seen in the BAL quasars.

The method for investigating the structure of the wind is basically the same used by Risaliti & Elvis (2010), but, based on the stellar wind theory, we employ a more realistic mass outflow rate proposed by Castor, Abbott, & Klein (1975) (hereafter CAK75). Furthermore, we perform higher resolution calculations and carefully treat the gas temperature and the ionization state to compare the model with wind properties inferred from the observations.

The steady structure of the disk winds is given by the calculation of the trajectories of fluid elements (streamlines), which are ejected from the surface of the geometrically thin and optically thick disks (Shakura & Sunyaev 1973). We solve the equation of motion considering the line force, coupling with the mass conservation along the streamline. We also calculate the temperature and the ionization parameter by taking account of the radiation transport of the X-ray from the vicinity of the black hole and UV emitted at the inner part of the disk. We show the schematic picture for our method in Figure 1. We calculate the streamlines in order of the distance from the black hole. When we solve i -th streamline, we take into consideration the extinction of the radiation via every inner streamline of j -th ($j < i$) as well as the self-shielding by i -th flow. We can obtain the global structure of the disk winds after calculating the final (outermost) streamline.

Next, we calculate the column density, the outward velocity, and the ionization parameter for a wide range of viewing angles and compare them with those inferred from X-ray observation of the BAL quasars. We evaluate the range of the viewing angle (i.e., the solid angle), at which our wind model is consistent with the observations. The solid angle divided by 4π means the probability that the system is identified as a BAL quasar (hereafter, BAL probability). We investigate the BAL probability for a variety of the black-hole mass and the Eddington ratio.

2.2. Initial conditions and basic equations

By solving the equation of motion including the radiation force, we investigate the trajectories (streamlines) of the fluid elements ejected from the disk surface in the cylindrical coordinates, (r, φ, z) . Here, the black holes and the accretion disk are located at the origin and the equatorial plane ($z = 0$). We assume the system to be axisymmetric with respect to the rotation axis.

The initial position (wind-base) of a fluid element is (r_0, z_0) . The first streamline starts at the innermost ra-

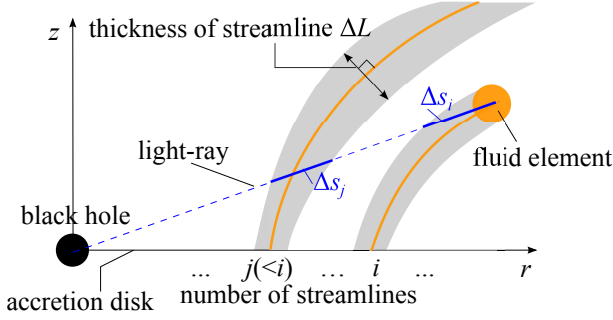


Fig. 1. Schematic picture for our calculation method. The black hole and the accretion disk are located at the origin and the equatorial plane ($z = 0$). Solid orange lines indicate the streamlines, and ΔL is the geometrical thickness of the each flow. The length of the light ray passing through the j -th flow is Δs_j . When we calculate the i -th streamline, the extinction of the radiation by inner streamlines (1st, 2nd, ..., $i-1$ th) and by the self-shielding of the i -th flow is taken into consideration.

radius of $r_0 = 20R_S$ (Here, we note that our results do not change so much if we employ $r_0 = 10R_S$). We calculate 81 streamlines by setting the interval of the initial points in r -direction to be $\Delta r_0 = 8R_S$ (We confirmed that the wind structure does not change significantly if we set the interval to be $\Delta r_0 = 2R_S$). That is, the initial radius of the i -th streamline is $20R_S + 8(i-1)R_S$, and the final fluid element is launched at the radius of $r_0 = 660R_S$. The initial altitude, z_0 , is set based on the hydrostatic balance in the vertical direction between the gravity and the pressure forces of gas and radiation, $GM_{BH}z_0/r_0^3 = c_s^2/z_0 + (\sigma_e/c)\sigma T_{eff}^4$, where G is the gravitational constant, c_s is the sound speed of the gas at the mid-plane ($z = 0$), σ_e is the mass-scattering coefficient for free electrons, c is the speed of light, σ is the Stefan-Boltzmann coefficient, and T_{eff} is the effective temperature. In the top panel of Figure 2, we show z_0 as a function of the distance from the black hole, r , normalized by R_S being the Schwarzschild radius, where we employ the alpha viscosity parameter of 0.1. We find z_0 depends on the black hole mass and the Eddington ratio (mass accretion rate).

At the wind base ($r = r_0, z = z_0$), we set the horizontal and azimuthal components of the velocity to be null and the Keplerian velocity. The initial density, ρ_0 , and the vertical component of the initial velocity, v_0 , are set so as to meet the prescription by CAK75, in which they investigated the steady and spherical wind driven by line force. The resulting mass outflow rate per unit surface at the distance of R is

$$\dot{m}_{CAK} = \frac{1}{\sigma_e v_{th}} \frac{GM_*}{R^2} \alpha (1-\alpha)^{(1-\alpha)/\alpha} \times (k\Gamma)^{1/\alpha} (1-\Gamma)^{-(1-\alpha)/\alpha}, \quad (1)$$

where v_{th} is the thermal speed of the gas, M_* is the mass of the star, α (~ 0.6) and k (~ 0.03) are the constants related to the line force, Γ is the Eddington ratio of the star [see equation (21) of CAK75]. By making minor revisions, we apply above relation to the mass outflow rate from the disk

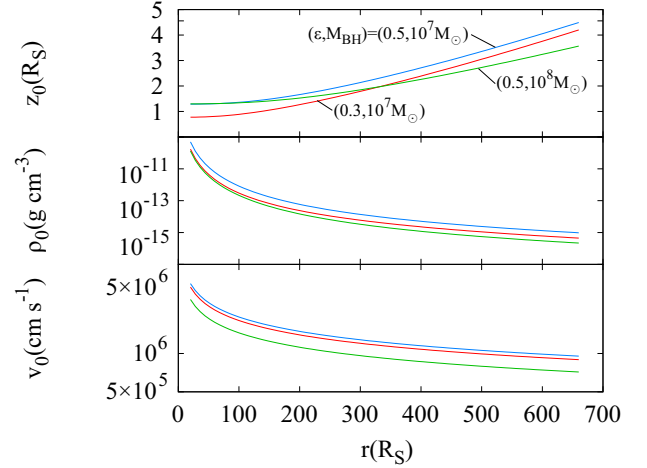


Fig. 2. The radial profile of the initial altitude (top panel), the initial density (middle panel), and the initial upward velocity (bottom panel) are plotted for $\epsilon = 0.3$ and $M_{BH} = 10^7 M_\odot$ (red line), for $\epsilon = 0.5$ and $M_{BH} = 10^7 M_\odot$ (blue line), and for $\epsilon = 0.3$ and $M_{BH} = 10^8 M_\odot$ (green line).

surface. The gravity GM_*/R^2 is replaced by $GM_{BH}z_0/r^3$, which is the gravity at the wind base. We use the local Eddington ratio,

$$\Gamma' = \frac{\sigma_e \sigma T_{eff}^4 / c}{GM_{BH}z_0/R^3} = \frac{3\epsilon}{4\eta z_0/R_S}, \quad (2)$$

as substitute for Γ . As a result, we have

$$\rho_0 v_0 = \frac{1}{\sigma_e v_{th}} \frac{GM_{BH}z_0}{r^3} \alpha (1-\alpha)^{(1-\alpha)/\alpha} \times (k\Gamma')^{1/\alpha} (1-\Gamma')^{-(1-\alpha)/\alpha}. \quad (3)$$

Throughout the present study, we assume the vertical component of the initial velocity to be the sound velocity at the disk surface, $v_0 = (k_B T_{eff} / \mu m_p)^{1/2}$, where k_B is the Boltzmann constant, μ ($= 0.5$) is the mean molecular weight, and m_p is the proton mass. Thus, the initial density, ρ_0 , is given by the equation (3). In Figure 2, we show ρ_0 (middle panel) and v_0 (bottom panel) as a function of r/R_S . Since v_0 is much smaller than the escape velocity, the disk wind appears if the fluid elements are accelerated by the line force.

Here we note that the density and velocity of the wind base are still unknown, although we apply the CAK75 relation. For instance, the mass outflow rate might be enhanced if the magnetic pressure force cooperates for launching the disk wind. High resolution radiation (magneto) hydrodynamic simulations would make clear the point.

The equation of motion including the radiation force is

$$\frac{d\mathbf{v}}{dt} = -\frac{GM_{BH}\mathbf{R}}{R^3} + \frac{l^2\mathbf{r}}{r^4} + \frac{\sigma_e(\mathbf{F}_{UV} + \mathbf{F}_X)}{c} + M \frac{\sigma_e\mathbf{F}_{UV}}{c}, \quad (4)$$

where $\mathbf{v} = (v_r, v_\phi, v_z)$ is the velocity, $R \equiv [(r^2 + z^2)^{1/2}]$ is the distance from the origin, \mathbf{R} is the point vector of the fluid element, l is the specific angular momentum, \mathbf{F}_X and \mathbf{F}_{UV} are the X-ray flux and the UV flux, and M is the

force multiplier (see below). The radiation force due to the free electrons is the third term of the right-hand side. The final term is line-driven radiation force, which may cause the disk wind in our model. The gas pressure is neglected.

Here, we speculate that the wind flow is launched from the disk surface perpendicularly, and is then directed away from the central source. When the flow is perpendicular to the disk plane, the geometrical thickness of each flow (ΔL , see Figure 1), which is measured at perpendicular to the streamline on r - z plane, is kept constant, $\Delta L = \Delta r_0$. If we simply assume $\Delta L \propto r$ when the wind is blown outward, the relation of $\Delta L = (r/r_0)\Delta r_0$ can describe the geometrical thickness of the flow both in the vertical and outward phases. Then, the density is given from the mass conservation equation ($2\pi r \Delta L \rho |v| = \text{const}$) as

$$\rho(v_r^2 + v_z^2)^{1/2} r^2 = \text{const}. \quad (5)$$

For comparison, we employ the other model, in which we assume the width of the flow does not broaden (the width is constant) not only when the flow is vertical to the disk, but also when the flow is blown outward; $\Delta L = \Delta r_0$. In this case, the density is estimated by $\rho(v_r^2 + v_z^2)^{1/2} r = \text{const}$. In the latter model, the density of the wind matter is relatively large at the distant region ($r \gg r_0$). Thus, the maximum of the ionization parameter becomes smaller. However, since the large fraction of the moderately ionized region appears where the flow is vertical to the disk ($r \sim r_0$), the BAL probability (see the §2.5) is nearly independent of the model of the wind geometry.

2.3. Radiative fluxes of X-ray and Ultraviolet

We consider two spectral components of the radiation, X-ray and UV. The luminosities of X-ray (L_X) and UV (L_{UV}) are given by $L_X = f_X \epsilon L_{\text{edd}}$ and $L_{UV} = (1 - f_X) \epsilon L_{\text{edd}}$. Here, f_X is the X-ratio, $L_X / (L_X + L_{UV})$, ϵ is defined as $\epsilon \equiv (L_X + L_{UV}) / L_{\text{edd}}$, and L_{edd} is the Eddington luminosity. In the present study, ϵ is a parameter and we employ $f_X = 0.15$.

X-ray is assumed to be emitted near the central black hole and treated as a central point source. The radial component (R -component) of the X-ray flux is written as

$$F_X^R = \frac{L_X}{4\pi R^2} e^{-\tau_X}, \quad (6)$$

where τ_X is the optical depth for X-ray measured from the origin. The other components of the X-ray flux are zero. We consider that the radiation is attenuated by the wind flow in the present study. When we calculate the i -th streamline, we take into consideration the obscuration by every inner streamline of j -th ($j < i$). That is, if a ray from the center to the fluid element gets across the j -th streamline ($j < i$), the radiation suffers from the dilution. Even if the ray does not get across, the j -th flow sometimes contributes to the obscuration because the flow has geometrical thickness (see §2.2). We also consider the self-shielding effect, which is extinction caused by the upper stream of the i -th flow. Therefore, the optical depth

is calculated by

$$\tau_X = \sum_{j \leq i} \Delta \tau_{X,j}, \quad (7)$$

where $\Delta \tau_{X,j} = \rho \sigma_X \Delta s_j$, with σ_X being the mass extinction coefficient for X-ray and Δs_j being the length that the ray passing through the j -th flow (see Figure 1). The mass extinction coefficient is defined by $\sigma_X = \sigma_e$ for $\xi \geq 10^5$ and $\sigma_X = 100\sigma_e$ for $\xi < 10^5$, where ξ is the ionization parameter defined as,

$$\xi [\text{erg cm s}^{-1}] = \frac{m_p L_X}{\rho R^2} e^{-\tau_X}. \quad (8)$$

This simple treatment of σ_X reflects that the photoelectric absorption is not effective when the ionization parameter is very high, since the number of bound electrons is too small (see also Risaliti & Elvis 2010). We have the r - and z -components of the X-ray flux is $F_X^r = F_X^R(r/R)$ and $F_X^z = F_X^R(z/R)$. The azimuthal component is zero.

We suppose that an optically thick and geometrically thin accretion disk is the only UV source where the effective temperature follows the radial profile of

$$T_{\text{eff}} = T_{\text{in}} \left(\frac{r}{r_{\text{in}}} \right)^{-3/4}, \quad (9)$$

where $r_{\text{in}} (= 3R_S)$ is the disk inner radius and T_{in} is the effective temperature at $r = r_{\text{in}}$. We set T_{in} so as to meet the condition of

$$(1 - f_X) \epsilon L_{\text{edd}} = \int_{r_{\text{in}}}^{r_{\text{out}}} 2\pi r \sigma T_{\text{eff}}^4 dr, \quad (10)$$

and the UV flux from the disk in the optically thin media is calculated by

$$F_{\text{thin}} = \int \frac{\sigma T_{\text{eff}}^4}{\pi} \mathbf{n} d\Omega, \quad (11)$$

where σ is the Stefan-Boltzmann coefficient, \mathbf{n} is the unit vector, and Ω is the solid angle. Here, note that we integrate the radiation of the disk within $r = r_{\text{out}}$, at which the effective temperature of the disk is 10^4 K, since the outer part is too cold to emit UV photons effectively, and since the disk luminosity of the outer part is much smaller than that of the inner part. For simplicity, we attenuate the radial component (R -component) of the UV flux using the optical depth measured from the origin, τ_{UV} , as

$$F_{UV}^R = F_{\text{thin}}^R e^{-\tau_{UV}}. \quad (12)$$

The numerical method for calculating τ_{UV} is the same as that for X-ray optical depth, but we use σ_e instead of σ_X . We assume that the dilution of the polar component of the UV flux is negligible,

$$F_{UV}^\theta = F_{\text{thin}}^\theta, \quad (13)$$

since the wind is expected to flow near the disk surface. The azimuthal component of the flux is zero by definition. In numerically, we divide the surface of the accretion disk into 256×256 small surface elements and calculate the UV flux.

2.4. Force multiplier

In order to estimate the line force, we employ the force multiplier proposed by Stevens & Kallman (1990), which is modified version of CAK75. The force multiplier, which is ratio of line force to electron-scattering force, is written as

$$M(t, \xi) = kt^{-0.6} \left[\frac{(1 + t\eta_{\max})^{0.4} - 1}{(t\eta_{\max})^{0.4}} \right], \quad (14)$$

Here, t is the local optical depth parameter

$$t = \sigma_e \rho v_{\text{th}} \left| \frac{dv}{ds} \right|^{-1}, \quad (15)$$

where $v_{\text{th}} = (k_B T / \mu m_p)^{1/2}$ is thermal velocity with T being the gas temperature, and dv/ds is the velocity gradient along the light-ray. Since k and η_{\max} depend on ξ as,

$$k = 0.03 + 0.385 \exp(-1.4\xi^{0.6}), \quad (16)$$

and

$$\log_{10} \eta_{\max} = \begin{cases} 6.9 \exp(0.16\xi^{0.4}) & \log \xi \leq 0.5 \\ 9.1 \exp(-7.96 \times 10^{-3}\xi) & \log \xi > 0.5 \end{cases}, \quad (17)$$

the force multiplier is the function of the local optical depth parameter, t , and the ionization parameter, ξ .

In our calculation, we approximate the velocity gradient

$$\frac{dv}{ds} = \frac{dv_1}{dl}, \quad (18)$$

where dv_1/dl is the velocity gradient along the streamlines. As we will show in Figure 3, the fluid element is lifted up in nearly vertical direction, since the vertical radiation flux from around the wind base mainly accelerate the matter upwards. Thus, the velocity gradient along the right-ray would be approximated by that along the streamlines. Subsequently, the matter is blown away in the radial direction. Then, the inner part of the accretion disk mainly illuminate the outflowing matter. Thus, above approximation would be valid.

We calculate the gas temperature assuming that the gas is in the radiative equilibrium, since the radiative cooling/heating timescale is much smaller than the cooling timescale via the adiabatic expansion (Proga et al. 2000),

$$n^2(G_{\text{Compton}} + G_X - L_{\text{b,l}}) = 0, \quad (19)$$

where, G_{Compton} is Compton heating/cooling rate,

$$G_{\text{Compton}} = 8.9 \times 10^{-36} \xi (T_X - 4T), \quad (20)$$

G_X is the rate of X-ray photoionization heating and recombination cooling,

$$G_X = 1.5 \times 10^{-21} \xi^{1/4} T^{-1/2} (1 - T/T_X), \quad (21)$$

$L_{\text{b,l}}$ is the bremsstrahlung and line cooling,

$$L_{\text{b,l}} = 3.3 \times 10^{-27} T^{1/2} + 1.7 \times 10^{-18} \xi^{-1} T^{-1/2} \times \exp(-1.3 \times 10^5/T) + 10^{-24}. \quad (22)$$

We assume the temperature of the X-ray radiation, $T_X = 10^8 \text{K}$, which is the same as Proga et al. (2000). Since this method for calculating the gas temperature is almost valid

in a low-density and high-ionization parameter regime, the gas temperature would be underestimated in the region of the high-density and low-ionization parameters. Thus, we set the lower limit of the gas temperature as being equal to the disk effective temperature, $T(r, z)_{\min} = T_{\text{eff}}(r)$.

Although, in the present work, the force multiplier depends on the gas temperature through the sound speed [see equation (14) and (15)], another model for the line force, which does not depends on the gas temperature, has been proposed by Gayley (1995). Our results does not change so much if we employ another force multiplier, since the gas temperature is kept around 10^4K in the region that the matter is mainly accelerated.

2.5. Assessment of BAL probability

A probability for observing BAL (BAL probability) is evaluated as follows. Using the resulting structure of the disk wind, we investigate the ionization parameter, the outward velocity, and the column density along lines of sight (from an observer to the central black hole). The X-ray observations of the BAL quasars reported the ionization parameter to be $\lesssim 500$ (Reeves et al. 2003, Gallagher et al. 2004) and several $\times 1000$ (Braitto et al. 2006, Wang et al. 2008). The X-ray observations also reveal that the outward velocity and the column density of the gas in such lower-ionization state are larger than 10^4km s^{-1} and larger than 10^{23}cm^{-2} (Chartas 2007 and references therein). Thus, we consider two conditions: (A) the outward velocity of the matter with $\xi < 100$ exceeds 10^4km s^{-1} and (B) the column density of the gas with $\xi < 100$ is larger than 10^{23}cm^{-2} . We also add the condition that (C) the column density is smaller than $1.5 \times 10^{24} \text{cm}^{-2}$, since the Compton thick objects would not be identified as BAL quasars. If three conditions are satisfied, we suppose that the X-ray absorption features emerge in the spectra. If this is the case, our wind model could also explain the BALs in UV band, since the X-ray absorption closely correlate to the BALs seen in UV wavelength (Brandt et al. 2000). We evaluate the solid angle, Ω_{BAL} , in which above conditions are satisfied. The BAL probability is given by $\Omega_{\text{BAL}}/4\pi$.

3. Results

3.1. Structure of line-driven wind

In Figure 3, red and black solid lines show trajectories of fluid elements (streamlines) ejected from the surface of the accretion disk in r - z plane. The mass of the black hole and the Eddington ratio, which are parameters in our calculation, are given as $M_{\text{BH}} = 10^7 M_{\odot}$ and $\epsilon = 0.3$ (hereafter, we call these 'baseline parameters'). The initial density, velocity, and altitude of streamlines are shown in Figure 2 (red lines). On the red lines, the matter is accelerated and attain a velocity equal to the escape velocity, $v = v_{\text{esc}}$ where $v = (v_r^2 + v_{\phi}^2 + v_z^2)^{1/2}$, at the points of the red filled circles. In contrast, the flow velocity does not reach the escape velocity on the black lines.

In the inner region, $r \lesssim 30 R_S$, it is found that the ejected fluid element immediately returns to the disk surface (we

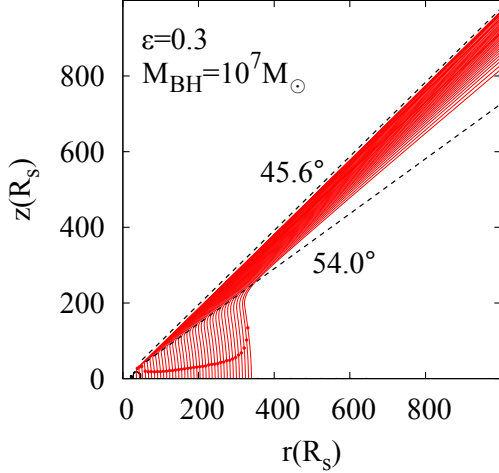


Fig. 3. The steady structure of the line-driven disk wind for $\epsilon = 0.3$ and $M_{\text{BH}} = 10^7 M_{\odot}$. The black hole and the accretion disk are located at the origin and the equatorial plane ($z = 0$). The red solid lines show trajectories of fluid elements (streamlines) ejected from the surface of the accretion disk. The red circles on the red lines indicate the point where the wind velocity exceeds the escape velocity. At the inner region of $r \lesssim 30R_s$, the ejected gas immediately goes back to the disk surface (black lines). It is also found that the wind is not launched at the outer region, $r > 350R_s$, although we can not see the streamlines in this figure. The BAL are observed at the viewing angle of $\theta = 45.6^\circ - 54.0^\circ$ (between dotted-lines).

call this 'failed wind') (see black lines). In this region, the initial density is too high for the line force to lift up the matter. High density reduces the ionization parameter because of $\xi \propto \rho^{-1}$ [see equation (8)]. Indeed, we have ξ is much less than 100 in this region. In the lower ionization regime ($\xi < 100$), the force multiplier decreases with an increase of the density, $M \propto \rho^{-0.6}$, since $M \propto t^{-0.6}$ where $t \propto \rho$ [see the equation (15)]. Therefore, the line force does not exceed the gravity and the gas is not blown away. Note that the mechanism of the failed wind in our work is different from that in previous works (Murray et al. 1995; Risaliti & Elvis 2010). We will discuss the point in section 4.2.

In the middle region, $30R_s \lesssim r \lesssim 350R_s$, we find that the disk wind is successfully launched. The matter launched from the disk surface is lifted up almost perpendicular to the disk plane, and exceeds the escape velocity (filled circles). Subsequently, such matter is blown away towards the direction with polar angle of $\theta \sim 45^\circ - 55^\circ$. The wind structure is understood as follows. Since the initial density ($\rho_0 \sim 10^{-14} - 10^{-13}$) is smaller in this region than in the inner region, and since the ionization parameter still less than 100, the force multiplier is large ($M \propto \rho^{-0.6}$), typically several $\times 100$. Thus, the vertical component of the radiation force (line force) is stronger than the that of the gravity. In contrast, the radiation from the vicinity of the black hole is attenuated by the failed wind, thus the radial component of the radiation force can not play an important role. As a consequence, the matter is accelerated in the vertical direction. Such a situation changes

Table 1. The BAL probability (%)

		Black hole mass (M_{BH}/M_{\odot})					
		10^7	$10^{7.5}$	10^8	$10^{8.5}$	10^9	$10^{9.5}$
Eddington ratio (ϵ)	0.9	7	7	7	5	0	0
	0.7	8	8	7	6	0	0
	0.5	9	9	8	8	0	0
	0.3	11	11	11	9	7	0
	0.01	0	0	0	0	0	0

at the region of $\theta \gtrsim 55^\circ$. The radiation from the inner accretion disk, which works to accelerate the matter outward, increase with a decrease of the polar angle and is not attenuated by the failed wind in the region. Therefore, outward radiation force bend the streamlines to radial direction and producing the funnel-shaped wind.

In the outer region beyond $r \sim 350R_s$, the temperature of the accretion disk is less than 10^4K and the disk around the wind base does not effectively emit UV photons. In addition, the UV radiation from the inner region of the accretion disk is obscured by the failed wind ($r \lesssim 30R_s$) and the disk wind ($30R_s \lesssim r \lesssim 350R_s$). Thus, although the initial density as well as the ionization parameter is small, the line force is made powerless and fails to form the wind.

According to the method mentioned in § 2.5, we investigate viewing angles for which the X-ray absorption features of the BAL quasars are observed. In the case of the disk wind with the baseline parameters, the conditions (A), (B), and (C) are satisfied at the viewing angle from $\theta = 45.6^\circ$ to 54.0° (see § 3.1). That is, then, the absorption features are observed, since the lower-ionization matter with sufficient radial velocity obscures the nucleus (see Figure 3). The BAL probability, $\Omega_{\text{BAL}}/4\pi$, is obtained as $\cos(45.6^\circ) - \cos(54.0^\circ) \sim 11\%$.

For the viewing angle smaller than 45.6° , there is no wind between the observer and the nucleus. When the viewing angle is between 54.0° and 63.0° , the column density is too large to detect the absorption features ($N_{\text{H}} > 1.5 \times 10^{24}\text{cm}^{-2}$), since the failed wind, of which the density is very high, obscures the nucleus. Thus, although the conditions (A) and (B) are satisfied, the object is not identified as the BAL quasars. For large viewing angle, $\theta > 63.0^\circ$, neither the condition (A) nor (C) is satisfied.

3.2. BAL Probability

Table 1 presents the BAL probability. For $\epsilon = 0.3 - 0.9$ and $M_{\text{BH}} = 10^{7-8.5}M_{\odot}$, we find that the BAL probabilities are 5–11% and are not so sensitive to the black hole mass as well as the Eddington ratio. On the other hand, the BAL quasars are not observed (BAL probability is null) in the case of $M_{\text{BH}} \gtrsim 10^9M_{\odot}$ or $\epsilon \lesssim 0.01$.

3.2.1. Eddington ratio dependence

For $\epsilon = 0.01$, the radiation is too weak to accelerate the matter. Since the wind is not successfully launched, the absorption features are not observed. The reason why the

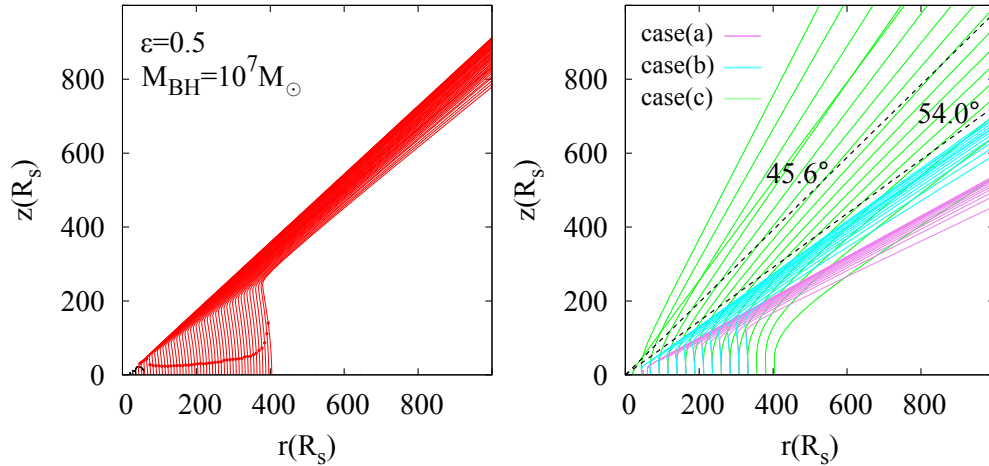


Fig. 4. Same as Figure 3, but for $\epsilon = 0.5$ (left panel). The disk structure is almost same with Figure 3, although the larger Eddington ratio is employed. The right panel is also the same as Figure 3, but we employ the initial altitude for $\epsilon = 0.5$ [case (a)], the initial density for $\epsilon = 0.5$ [case (b)], and the disk luminosity for $\epsilon = 0.5$ [case (c)]. The larger initial altitude and density work to increase the opening angle of the funnel-shaped wind. In contrast, the larger luminosity tends to accelerate the matter upward.

BAL probability is roughly kept constant for $\epsilon = 0.3 - 0.9$ and $M_{\text{BH}} = 10^{7-8.5} M_{\odot}$ is understood by the left panel in Figure 4. This panel is the same as the Figure 3, but for $\epsilon = 0.5$. It is found that the wind launching region broadens as an increase with ϵ . However, we find that the opening angle and the thickness of the funnel-shaped wind does not change so much. Therefore, the BAL probability is roughly independent of the Eddington ratio.

Since the initial values and the disk luminosity changes with ϵ , here, we at first consider an influence of the initial density on the wind structure. For this purpose, we employ the initial density profiles for $\epsilon = 0.5$ (blue line of the middle panel in Figure 2), but other initial conditions and the disk luminosity are set to the values for $\epsilon = 0.3$ (red lines of the top and bottom panels in Figure 2). The result is plotted by purple lines in the right panel of Figure 4 [case (a)]. We find that the resulting disk wind has an wide opening angle ($\theta \sim 65^\circ$). Since the initial density increases as an increase of ϵ (see Figure 2), and since the line force is less effective for the gas with large density ($M \propto \rho^{-0.6}$, see §3.1), the height of the failed wind is small and the stream lines of the disk wind bends at the small altitude for the case (a) in comparison with the case with baseline parameter. We conclude that the higher density tends to make the opening angle of the disk wind larger.

Next, we consider an effect of the initial altitude, z_0 . The blue lines of the right panel of Figure 4 show the result for the case (b) in which the initial altitude for $\epsilon = 0.5$ (blue line of the top panel in Figure 2) is supposed, although the luminosity, initial density and velocity remain the values for $\epsilon = 0.3$ (red lines of middle and bottom panels in Figure 2). That is, the larger z_0 is employed in comparison with the case with the baseline parameters. Then, since the initial position is distant from the disk surface, the radiation force becomes less effective relatively and the disk wind with the large opening angle is generated. As we have discussed above, the less effective radiation

force works to form the lower failed wind, leading to the disk wind with larger opening angle.

The large disk luminosity tends to narrow the opening angle. The green lines [case (c)] show the streamlines when the radiation fields are calculated by assuming $\epsilon = 0.5$ and other initial conditions remain the values for $\epsilon = 0.3$ (red lines in Figure 2). Comparing with the streamlines for $\epsilon = 0.3$ (Figure 3), the matter, which is launching at $r < 150 R_{\text{S}}$, is blown away more upward, inducing the small opening angle of the funnel-shaped wind. This is because the UV radiation is strong and the line force effectively accelerates the matter. We also find that the wind is launching from wide region of the disk, $r < 400 R_{\text{S}}$, since the UV emitting region ($T_{\text{eff}} \geq 10^4 \text{K}$) expands with an increase of ϵ .

To sum up, the increase of the luminosity, which contributes to reduce the opening angle of the wind, counteracts the increase of the initial density and altitude, which works to expand the funnel. As a result, the BAL probability is insensitive to the Eddington ratio for $\epsilon = 0.3 - 0.9$ and $M_{\text{BH}} = 10^{7-8.5} M_{\odot}$. Here, we note that the initial velocity has little influence on the wind structure. Indeed, we verified that the wind structure does not change if the initial velocity for $\epsilon = 0.5 - 0.9$ is employed.

3.2.2. Black hole mass dependence

The BAL probability is insensitive to the black hole mass for $M_{\text{BH}} = 10^{7-8.5} M_{\odot}$, but tends to be null for $M_{\text{BH}} \gtrsim 10^9 M_{\odot}$. Figure 5 shows the streamlines for $M_{\text{BH}} = 10^8 M_{\odot}$ and $\epsilon = 0.5$. This figure shows that the opening angle for $M_{\text{BH}} = 10^8 M_{\odot}$ is comparable to or slightly smaller than that for $M_{\text{BH}} = 10^7 M_{\odot}$. We also find that the launching region, which is measured in an unit of R_{S} , shrinks with an increase of the black hole mass. Such behavior is caused by the decrease of the force multiplier as well as the temperature of the disk.

The local optical depth parameter, $t = \sigma_e v_{\text{th}} \rho (dv_l/dl)^{-1}$, is roughly evaluated as $t = \sigma_e \rho_0 z_0$ near the wind base,

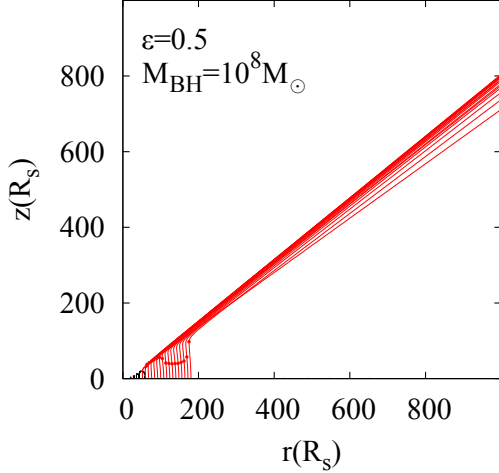


Fig. 5. Same as the left panel of Figure 4, but for $M_{\text{BH}} = 10^8 M_{\odot}$. The half opening angle of the wind does not depend on the black hole mass. However, the wind launching region shrinks with an increase of the black hole mass.

where we suppose $v_{\text{th}} \sim v_0$, $\rho \sim \rho_0$, and $dv_l/dl \sim v_0/z_0$. Since z_0 is roughly proportional to M_{BH} ($z_0 \propto R_s$), Γ' is almost independent from the black hole mass (see equation 2). We have $\rho_0 \propto (1/v_0^2)(M_{\text{BH}}^2/r^3) \propto M_{\text{BH}}^{-3/4}$ with using the relation of $v_0 \propto M_{\text{BH}}^{-1/8}$. Thus, the optical depth parameter is proportional to $M_{\text{BH}}^{1/4}$, and we have a very weak M_{BH} -dependence of the force multiplier, $M \propto t^{-0.6} \propto M_{\text{BH}}^{-0.15}$. As we have discussed above, the disk wind with the wide opening angle form since the force multiplier is small (radiation force is less effective). Thus, the opening angle for $M_{\text{BH}} = 10^8 M_{\odot}$ is comparable to or slightly larger than that for $M_{\text{BH}} = 10^7 M_{\odot}$.

The size of the UV emitting region of the accretion disk ($T_{\text{eff}} > 10^4 \text{K}$), which is normalized by R_s , is proportional to $M_{\text{BH}}^{-1/3}$, in the case that the Eddington ratio is kept constant. This is the main reason that the launching region of the wind becomes small when the black hole is massive.

Since the UV emitting region becomes narrowed, and since the failed wind region slightly expands via the reduction of the line force ($M \propto M_{\text{BH}}^{-0.15}$), the disk wind tends to disappear when the black hole is too massive ($M_{\text{BH}} \gtrsim 10^9 M_{\odot}$). Hence, it is implied that the absorption features are not identified in the quasars with very massive black holes.

4. Discussion

4.1. Comparison with observations

Our model indicates that the BAL probability is several to 10 percent for a wide range of the Eddington ratio and the black hole mass, $\epsilon = 0.3 - 0.9$ and $M_{\text{BH}} = 10^{7-8.5} M_{\odot}$. This result is roughly consistent with the abundance ratio of BAL quasars, $\sim 10 - 20\%$ (e.g., Allen et al. 2011). The resulting BAL probability might increase, if the nucleus is obscured by the dusty torus, which aligns with the ac-

cretion disk, is not identified as quasars. For instance, the BAL probability is doubled, $10 - 20\%$, if the observer with $\theta \geq 60^\circ$ cannot detect quasars via the obscuration by the thick torus. Even if that is the case, our result is consistent with the abundance ratio.

In this regime of $\epsilon = 0.3 - 0.9$ and $M_{\text{BH}} = 10^{7-8.5} M_{\odot}$, our model indicates that the observer's viewing angle is responsible for the difference between BAL and non-BAL quasars. If the observer is in the direction of the wind flow the absorption features are detected. Otherwise, the nuclei are identified as non-BAL quasars. That is, our result gives physical bases in phenomenological model (Elvis 2000), in which the dichotomy between the BAL and non-BAL quasars is explained by the observer's viewing angle. Note that, in addition to such a viewing-angle effect, our results imply that the BAL features does not appear if the Eddington ratio is too small ($\epsilon \lesssim 0.01$) or if the black holes is too massive ($M_{\text{BH}} \gtrsim 10^9 M_{\odot}$).

Here, we note that our model overestimate the BAL probability in the regime of $\epsilon = 0.05 - 0.1$. Although our model gives the probability of $20 - 50\%$, the accurate value would be much small. The launching matter is blown away for a wide angle for $\epsilon = 0.05 - 0.1$, leading to the larger BAL probability. The streamlines for $\epsilon = 0.1$ is plotted in Figure 6. In this case, the BAL probability is 48 %. However, then, the mass outflow rate of the wind is a few times larger than the mass accretion rate of the disk. This implies that our model overproduces the outflows, and actual BAL probability should be smaller than 48 %. In the case that the mass accretion rate is comparable to the mass outflow rate, we need to solve the outflow and the disk, self-consistently (we will discuss later).

4.2. Comparison with previous works

Throughout the present study, we employ the non-hydrodynamic method that is basically the same with that used in Risaliti & Elvis (2010). In Risaliti & Elvis (2010), the initial density and velocity are treated as free parameters and assumed to be constant in the radial direction, for simplicity. However, we employ more realistic profiles of ρ_0 and v_0 based on CAK75, in which the mass outflow rate of the line-driven stellar wind is investigated in detail. Such a discrepancy of the initial values leads to the difference of the wind structure. In Risaliti & Elvis (2010), since the matter is overionized by X-ray irradiation at the vicinity of the black hole, the line force is made powerless and fails to launch the wind. Murray et al. (1995) also reported that the failed wind appears in the vicinity of the black hole via X-ray irradiation. In our work, the matter is not highly ionized via the high density (see ρ_0 profiles in Figure 2). However, high density reduces the force multiplier and prevents the launching of the wind as we have mentioned in section §3.1. Also, the outer part of the disk contributes more to the total mass loss rate ($\propto \rho_0 v_0 r^2$) than the inner disk in Risaliti & Elvis (2010), since ρ_0 and v_0 are constant in the radial direction. In contrast, ρ_0 as well as v_0 increase with the decrease of r , meaning that the disk loses more mass from the inner part of the launching region.

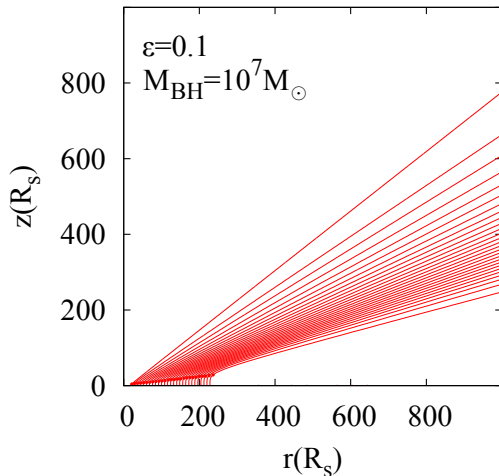


Fig. 6. Same as Figure 3, but for $\epsilon = 0.1$. In this case, the wind with large covering factor forms.

Here, we note that the wind structure calculated by the present non-hydrodynamic method is similar to that calculated by hydrodynamic simulations of PK04. The opening angle of the wind, $\sim 60^\circ$, for PK04 approximately coincides with our result, $\sim 50^\circ$. The column density of the wind in the moderate or low ionization state is around $10^{24-25} \text{cm}^{-2}$ ($\theta \sim 70^\circ$) in PK04, and $10^{24-25} \text{cm}^{-2}$ ($\theta \sim 60^\circ$) and $\gtrsim 10^{25} \text{cm}^{-2}$ ($\theta \gtrsim 70^\circ$) in our model. The wind velocity is much larger in our work than in PK04. The outward velocity is $100,000 \text{km s}^{-1}$ in our work, but PK04, on the other hand, showed around $10,000 \text{km s}^{-1}$ (the peak value is $20,000 \text{km s}^{-1}$). Such a discrepancy is though to be caused by that the disk wind is launched from more inner region in our model than in PK04. In PK04, as well as Risaliti & Elvis (2010), the density just above the disk surface is set to be constant in the radial direction. Thus, the density at the wind base is lower in PK04 than in our model at the inner region. The less dense matter is almost fully ionized and is not accelerated by line force. The failed wind region in PK04 is larger than that in our model. The wind launched from the inner region is effectively accelerated by strong UV radiation from the inner part of disk, leading to higher velocity of the wind. Here we comment that, when the initial density is set to be the same as that in PK04, we can approximately reproduce the results of PK04, e.g., the wind velocity of $10,000 \text{km s}^{-1}$ and the failed wind due to overionization.

Feldmeier et al. (1999) investigated the line driven wind in cataclysmic variables. Their streamlines are almost in parallel with each other. Such a feature is similar with our results. However, they reported that the opening angle of the wind is $10^\circ - 30^\circ$, which is much smaller than that of our model and PK04, $50^\circ - 60^\circ$. Although the streamlines bend above the disk in our model, straight lines are assumed in Feldmeier et al. (1999). Also, the dilution of the radiative flux by the wind (self-shielding) is not taken into consideration in Feldmeier et al. (1999).

4.3. Future work

Although axisymmetric hydrodynamic simulations of the line-driven wind are attempted by PK00 and PK04, three-dimensional hydrodynamic approaches would be important future work. Recently, the time variation of the absorption features has been reported by Misawa et al. (2007). This implies that the wind structure changes with time and/or non-axisymmetric pattern exists in the winds. Such problems would be resolved by three-dimensional hydrodynamic simulations. Owocki & Puls (1999) have reported using one-dimensional calculations that the line-driven wind exhibits violent density fluctuations and many density peaks. In addition, Proga et al. (2000) and PK04 have shown that high density blobs are sometimes generated in the wind. However, their work is a two-dimensional study. We will explore the three-dimensional simulations to investigate the time evolution and non-axisymmetric structure of the winds.

In the case that the mass outflow rate is comparable to the mass accretion rate of the disk, we should solve the wind and disk, self-consistently. The wind extracts the mass, angular momentum, and the energy from the disk. The disk structure, thus, changes via launching of the wind, and the wind structure is subject to influence of the changing the disk structure. As we have discussed above, the mass outflow rate is comparable to or larger than mass accretion rate for $\epsilon = 0.05 - 0.1$ in our model. By X-ray observations of AGNs, Tombesi et al. (2012) reported that the mass outflow rate via the ultra fast outflows is comparable to the mass accretion rate onto the black hole.

In the present study, we verify the line-driven wind model based on the ionization parameter, the outward velocity, and the column density. However, we should calculate the emergent spectra and directly compare these with the observations. Such a study was recently attempted by Sim et al. (2010), in which they performed Monte Carlo radiative transfer simulations in the X-ray band.

5. Conclusions

We have studied the structure of the disk wind driven by the radiation force including the line force, by calculating trajectories of the fluid elements which are launched from the surface of the geometrically thin and optically thick disk. Here, the density and velocity at the wind base are set so as meet the condition of line-drive stellar wind (CAK75). We have solved the equation of motion, coupling with the mass conservation along the streamlines. The radiation force, the ionization parameter, and the temperature are calculated by taking into consideration the extinction of the X-ray from the vicinity of the black hole and the UV from the disk by the ejected matter. We have compared the resulting wind structure with the wind properties of X-ray observations of the BAL quasars (the ionization parameter, the outward velocity, and the column density), and estimated the probability (BAL probability), with which the system is identified as a BAL quasar.

In the case that the Eddington ratio is $\varepsilon \sim 0.3 - 0.9$ and the black hole mass is $M_{\text{BH}} \sim 10^{7-8.5} M_{\odot}$, we found that the funnel-shaped disk wind with a opening angle of $\sim 50^\circ$ forms. In this regime, since the wind shape is insensitive to the Eddington ratio and the black hole mass, the BAL probability of several to 10 percent does not change so much. The observer's viewing angle is responsible for whether or not the quasars exhibit the broad absorption lines. Our model is consistent with the phenomenological model of BAL quasars proposed by Elvis (2000).

The wind is launched from the middle region of the disk, where the line force is strong enough to accelerate the matter. At the inner region, since the larger initial density reduces the force multiplier (line force), the ejected matter immediately returns to the disk surface. On the other hand, in the outer region, since the UV radiation is attenuated via the obscuration by the matter in the inner and middle regions, the radiation force fail to launch the wind. In the case of $M_{\text{BH}} = 10^7 M_{\odot}$ and $\epsilon = 0.3$, the launching region is $30R_{\text{S}} \lesssim r \lesssim 350R_{\text{S}}$.

If the Eddington ratio is very small ($\varepsilon \lesssim 0.01$), the disk wind does not appear, since the UV intensity is too weak for the matter to be accelerated by the line force. Also, the disk wind is not launched when the black hole is too massive ($M_{\text{BH}} \gtrsim 10^9 M_{\odot}$). This is because that the force multiplier at the wind base decreases with an increase of the black hole mass. In addition, the disk temperature also decreases (UV emission region, $T_{\text{eff}} > 10^4 \text{K}$, shrinks) with an increase of the black hole mass. Thus, for $\varepsilon \lesssim 0.01$ or for $M_{\text{BH}} \gtrsim 10^9 M_{\odot}$, the BAL quasars are not observed independently of the viewing angle.

We would like to thank Masahiro Morikawa and Yoshito Haba for useful discussions. This work is supported in part by the Ministry of Education, Culture, Sports, Science, and Technology (MEXT) Young Scientist (B) 20740115 (K.O.), 21740150 (T. M.), and Scientific Research (C) 23540267 (K. W.), 22540295 (H. S.).

References

Allen, J. T., Hewett, P. C., Maddox, N., Richards, G. T., & Belokurov, V. 2011, *MNRAS*, 410, 860
 Blandford, R. D., & Payne, D. G. 1982, *MNRAS*, 199, 883
 Braitto, V., et al. 2006, *Astronomische Nachrichten*, 327, 1067
 Brandt, W. N., Laor, A., & Wills, B. J. 2000, *ApJ*, 528, 637
 Castor, J. I., Abbott, D. C., & Klein, I. 1975, *ApJ*, 195, 157
 Chartas, G. 2007, *Spectral Line Shapes in Astrophysics*, 938, 3
 Elvis, M. 2000, *ApJ*, 545, 63
 Everett, J. E., & Murray, N. 2007, *ApJ*, 656, 93
 Feldmeier, A., Shlosman, I., & Vitello, P. 1999, *ApJ*, 526, 357
 Foltz, C. B., Weymann, R. J., Morris, S. L., & Turnshek, D. A. 1987, *ApJ*, 317, 450
 Gallagher, S. C., Brandt, W. N., Wills, B. J., Charlton, J. C., Chartas, G., & Laor, A. 2004, *ApJ*, 603, 425
 Gayley, K. G. 1995, *ApJ*, 454, 410
 Hamann, F., Korista, K. T., & Morris, S. L. 1993, *ApJ*, 415, 541
 Jannuzi, B. T., et al. 1996, *ApJL*, 470, L11

Konigl, A., & Kartje, J. F. 1994, *ApJ*, 434, 446
 Misawa, T., Eracleous, M., Charlton, J. C., & Kashikawa, N. 2007, *ApJ*, 660, 152
 Murray, N., Chiang, J., Grossman, S. A., & Voit, G. M. 1995, *ApJ*, 451, 498
 Owocki, S. P., & Puls, J. 1999, *ApJ*, 510, 355
 Proga, D., Stone, J. M., & Drew, J. E. 1998, *MNRAS*, 295, 595
 Proga, D., Stone, J. M., & Drew, J. E. 1999, *MNRAS*, 310, 476
 Proga, D., Stone, J. M., & Kallman, T. R. 2000, *ApJ*, 543, 686
 Proga, D., & Kallman, T. R. 2004, *ApJ*, 616, 688
 Reeves, J. N., O'Brien, P. T., & Ward, M. J. 2003, *ApJL*, 593, L65
 Risaliti, G., & Elvis, M. 2010, *A&A*, 516, 89
 Shakura, N. I., & Sunyaev, R. A. 1973, *A&A*, 24, 337
 Schurch, N. J., Done, C., & Proga, D. 2009, *ApJ*, 694, 1
 Sim, S. A., Proga, D., Miller, L., Long, K. S., & Turner, T. J. 2010, *MNRAS*, 408, 1396
 Stevens, I. R., & Kallman, T. R. 1990, *ApJ*, 436, 599
 Tombesi, F., Cappi, M., Reeves, J. N., & Braitto, V. 2012, *MNRAS*, 422, L1
 Wang, J., Jiang, P., Zhou, H., Wang, T., Dong, X., & Wang, H. 2008, *ApJL*, 676, L97
 Weymann, R. J., Morris, S. L., Foltz, C. B., & Hewett, P. C. 1991, *ApJ*, 373, 23